Use of WRF-Hydro to Simulate Runoff-Generated Debris Flow Hazards in Burn Scars

C. Li[1], A. L. Handwerger[2,3], J. Wang[4], W. Yu[5,6], X. Li[7], N. J. Finnegan[8], Y. Xie[9,10], G. Buscarnera[7], and D. E. Horton[1]

[1] Department of Earth and Planetary Sciences, Northwestern University

[2] Joint Institute for Regional Earth System Science and Engineering, University of California, Los Angeles, CA, 90095, USA

[3] Jet Propulsion Laboratory, California Institute of Technology, Pasadena, CA, 91109, USA

[4] Environmental Science Division, Argonne National Laboratory, Lemont, IL, 60439, USA

[5] Cooperative Institute for Research in Environmental Sciences, University of Colorado Boulder

[6] NOAA/Global Systems Laboratory, 325 Broadway, Boulder, Colorado

[7] Department of Civil and Environmental Engineering, Northwestern University

[8] University of California Santa Cruz, Department of Earth and Planetary Sciences, Santa Cruz, CA, 95064, USA

[9] Program in Environmental Sciences, Northwestern University, 2145 Sheridan Road, Evanston, IL, 60208, USA

[10] Department of Biological Sciences, Purdue University, 915 W State St, West Lafayette, IN 47907, USA

Corresponding author: Chuxuan Li (chuxuanli2020@u.northwestern.edu)

Key Points:

- WRF-Hydro is modified to output overland flow for use in postfire flooding and debris-flow hazard assessments.
- Debris-flow hazard potential of the January 2021 atmospheric river on the Dolan burn scar in California, USA is simulated.
- Adding burn scar characteristics alters discharge timing and increases overland and peak channel discharge, improving simulated hydrograph.

Abstract

Between 26–29 January 2021 an atmospheric river (AR) triggered numerous debris flows within the 2020 Dolan wildfire burn scar in Big Sur, California. Here we modify WRF-Hydro to simulate both overland and channelized flows and assess the potential for runoff-generated debris-flow hazards in burn scars. High-resolution weather radar-derived precipitation is used to drive baseline and burn scar sensitivity experiments. Compared to the baseline, the burn scar simulation yields dramatic increases in total and peak discharge, as well as shorter lags between rainfall onset and peak discharge. At Rat Creek, where California Highway 1 was destroyed, discharge volume increased eight-fold and peak discharge tripled relative to the baseline. Our WRF-Hydro-based hazard assessment indicates that over 1/3 of Dolan burn scar catchments were under "very high" debris-flow hazards. Our work demonstrates that a modified version of WRF-Hydro provides a compelling new physics-based tool to investigate and potentially predict postfire hydrologic hazards.

Plain Language Summary

In January of 2021 a winter storm triggered numerous debris flows in the mountains of coastal California in an area that had recently been burned by wildfire. One of the debris flows destroyed California's famous Highway 1 – substantially impacting local residents and severely curtailing tourism. Here we use a hydrologic model to assess the hazard potential for debris flows in the area, as well as constrain the change in debris-flow hazard that resulted from wildfire-induced changes to the land surface. We use high-resolution meteorological data to drive simulations under pre-fire and postfire scenarios. Compared to the pre-fire model run, the postfire simulation yields dramatic increases in total and peak discharge, as well as shorter lags between rainfall onset and peak discharge. Our model simulation hazard assessment indicates that over 1/3 of the basins within the burn scar were under "very high" debris-flow hazards. Our work demonstrates the utility of three-dimensional hydrologic models for investigating debris-flow hazards and suggests these tools might one day be used to forecast postfire hydrologic hazards.

1 Introduction

Following intense rainfall, areas with wildfire burn scars are more prone to flash flooding (Neary et al., 2003; Bart & Hope 2010; Bart 2016) and runoff-generated debris-flow hazards compared to unburned areas (Moody et al., 2013; Ice et al., 2004; Shakesby & Doerr, 2006). After wildfire, reduced tree canopy interception, decreased soil infiltration due to soil-sealing effects (Larsen et al., 2009), and increased soil water repellency – especially in hyper-arid environments (Dekker and Ritsema, 1994; Doerr and Thomas, 2000; MacDonald and Huffman, 2004) – increases excess surface water, and on sloped terrains leads to overland flow (Shakesby & Doerr, 2006; Stoof et al., 2012). As water moves down hillslopes and erosion adds sediment to water-dominated flows, clear

water floods can transition to turbulent and potentially destructive debris flows (Meyer & Wells, 1997; Cannon et al., 2001, 2003; Santi et al., 2008). In contrast to debris flows initiated by shallow landslides, this rainfall-runoff process has been identified as the major cause for postfire debris flows in the western U.S. (Cannon, 2001; Cannon et al., 2003, 2008; Kean et al., 2011; Nyman et al., 2015). In California, because climate change is projected to increase the intensity and frequency of wet-season precipitation (Swain et al., 2018; Polade et al., 2017), increase wildfire potential (Swain, 2021; Brown et al., 2021), and extend the wildfire season (Goss et al., 2020) occurrence and intensity of postfire debris flows are likely to increase (Cannon et al., 2009; Kean & Staley, 2021; Oakley, 2021).

To predict postfire debris-flow hazards, statistical approaches are commonly used. For example, the United States Geological Survey (USGS) uses logistic regression models to predict the likelihood of post-wildfire debris flows (Staley et al., 2016; Cannon et al., 2010) and multiple linear regression models to predict debris-flow volumes (Gartner et al., 2014). However, statistical approaches do not simulate underlying physics, limiting the understanding of debris-flow mechanisms. Physics-based models that simulate spatially-explicit hydrologic and mass wastage processes are well-suited for sensitivity analyses, but applications of these models often focus on landslide-induced debris flows (e.g., Iverson & George, 2014; George & Iverson, 2014), rather than runoff-generated debris flows which are more common in postfire areas (Cannon et al., 2001, 2003; Santi et al., 2008). Studies that have used process-based models to investigate postfire hydrologic responses have focused on triggering mechanisms of postfire debris flows at high spatiotemporal resolutions (McGuire et al., 2017) and long-term runoff responses at coarse temporal resolutions (Rulli & Rosso, 2007; McMichael & Hope 2007). To overcome computational limits process-based models often adopt simplifications that can limit effective prediction and hypothesis testing. For example, the kinematic runoff and erosion model (KINEROS2) simplifies drainage basins into 1-dimensional channels and hillslope patches (Canfield & Goodrich, 2005; Goodrich et al., 2012; Sidman et al., 2015), and the Hydrologic Modeling System (HEC-HMS) uses an empirically-based curve number method to estimate saturation excess water (Cydzik et al., 2009), which cannot resolve infiltration excess overland flow, a critical process in burn scars (Chen et al., 2013).

Here we explore use of the physics-based and fully-distributed Weather Research and Forecasting Hydrological modeling system version 5.1.1 (WRF-Hydro) to assess hazard potential in burn scars. WRF-Hydro is the core of National Oceanic and Atmospheric Administration's (NOAA) National Water Model forecasting system and has been used extensively to study channelized flows (e.g., Lahmers et al., 2020; Wang et al., 2019). Here, we modify WRF-Hydro to output high temporal resolution fine-scale (100 m) debris flow-relevant overland flow; a process computed using a fully unsteady, explicit, finite difference diffusive wave formulation. Previous efforts, employing diffusive, kinematic, and diffusive-kinematic wave models, have demonstrated that water-only models can provide critical insights on runoff-driven debris flow behavior (Arattano & Savage, 1994; McGuire & Youberg, 2020; Arratano & Franzi, 2010; Di Cristo et al., 2021), even in burned watersheds (Rengers et al., 2016).

To demonstrate the utility of WRF-Hydro in debris flow studies, we investigate the January 2021 debris flow events within the Dolan burn scar on the Big Sur coast of central California. We first identify multiple debris flow sites using optical and radar remote sensing data and field investigations. We then calibrate WRF-Hydro against ground-based hydrologic observations and use it to study the effects of burn scars on debris-flow hydrology and changes in hazard potential.

2 Background of case study

The Dolan wildfire burned from August 18th till December 31st, 2020. 55% of areas within the fire perimeter were burned at moderate-to-high severity (Burned Area Emergency Response, 2020). After the fire, USGS Emergency Assessment of Post-Fire Debris-Flow Hazards produced a debris-flow hazard assessment using a design storm based statistical model (USGS, 2020). On January 26–29, 2021, an atmospheric river (AR) made landfall on the Big Sur coast, bringing more than 300 mm of rainfall to California's Coast Ranges (Figure S1), with a peak rainfall rate of 240 mm/hr. During the AR event, a section of California State Highway 1 (CA1) at Rat Creek was destroyed by a debris flow. CA1 was subsequently closed for three months and rebuilt at a cost of ~$11.5M (Los Angeles Times, 2021).

2.1 Debris flow identification from remote sensing and field work

In addition to the Rat Creek debris flow, which made national news, we identified three other debris flows using a combination of field investigation, and open access satellite optical and synthetic aperture radar (SAR) images (Figure S2; Supporting Information Text S1). We examined satellite optical images collected by Copernicus Sentinel-2 (S2) satellites in the cloud-based Google Earth Engine (GEE). We also examined relative differences in normalized difference vegetation index (rdNDVI) calculated from S2 data using the HazMapper GEE application (Scheip & Wegmann, 2021), which identifies areas where vegetation was lost due to debris flows (and other causes). Lastly, we analyzed changes in SAR backscatter data from Copernicus Sentinel-1 (S1) satellites by comparing pre- and post-event SAR images in GEE (Handwerger et al., in review). Identified debris-flow source areas and deposition sites were confirmed by field investigation (N.J. Finnegan) and named after the locations where they deposited (i.e., Big Creek, Mill Creek, and Nacimiento). We note that there were likely more debris flows triggered during the AR event. However, given the primary goal of this study – to demonstrate the utility of WRF-Hydro – a comprehensive cataloging of debris flows is beyond this study's scope.

3 WRF-Hydro

3.1 Model description

WRF-Hydro is an open-source physics-based community model that simulates land surface hydrologic processes. It includes the Noah-Multiparameterization (Noah-MP) land surface model

(LSM; Niu et al., 2011), terrain routing module, channel routing module, and a conceptual baseflow bucket model. Noah-MP LSM is a 1-D column model that calculates surface and subsurface runoff on the LSM grid (1 km), while terrain and channel routing modules simulate overland flow and streamflow on a finer terrain routing grid (100 m).

By default, soil hydraulic and land surface properties are functions of soil texture and land cover types in WRF-Hydro (Supporting Information Text S2, Figures S3&S4, and Tables S1&S2).

3.2 Meteorological forcing files

WRF-Hydro is used in standalone mode (i.e., no coupling with atmospheric model) and forced with a combination of Phase 2 North American Land Data Assimilation System (NLDAS-2) meteorological data and Multi-Radar/Multi-Sensor System (MRMS) radar-only quantitative precipitation. NLDAS-2 provides hourly forcing data including incoming shortwave and longwave radiation, 2-m specific humidity and air temperature, surface pressure, and 10-m wind speed at 1/8-degree spatial resolution. MRMS provides hourly precipitation rate at 1-km resolution.

3.3 Simulation and output of overland flow

The Noah-MP LSM calculates infiltration excess (governing equations in Supporting Information Text S3) and passes excess water to the terrain routing module, which then simulates overland flow using a fully-unsteady, explicit, finite-difference diffusive wave equation adapted from Julien et al. (1995) and Ogden (1997). If overland flow intersects grid cells identified as channel grids (2^{nd} Strahler stream order and above; pre-defined by the hydrologically conditioned USGS National Elevation Dataset 30-m digital elevation model (DEM)), the channel routing module routes the water as channelized streamflow.

Off-the-shelf, WRF-Hydro does not output overland flow at terrain routing grids (100 m), however it is computed in the background to determine channelized streamflow. We modified WRF-Hydro source code to output overland flow. Overland flow depth (m) was converted to overland discharge (m^3/s) by multiplying flow depth by grid cell area (10,000 m^2) and dividing by the LSM time step (1 hr).

4 Model simulation, calibration, and validation

4.1 Model domain

The model domain spans the Coast Ranges of central California, Monterey Bay, and the Central Valley, and covers several burn scars from the 2020 wildfire season (Figure 1a). Here we focus our analysis on the Dolan burn scar (Figure 1b). According to the USGS 30-m DEM, the Rat Creek debris-flow site sits at the base of a 1^{st} order catchment with a drainage area of 2.23 km^2. Mill Creek, Big Creek, and Nacimiento debris flows were initiated within extremely steep, intensely burned, 1^{st} order catchments, but were deposited in 2^{nd}, 3^{rd}, and 3^{rd} Strahler stream order channels,

respectively. We calibrated and validated WRF-Hydro output using the 2-minute soil moisture observations from two Physical Sciences Laboratory (PSL) monitoring stations (i.e., Lockwood (lwd) and Gilroy (gry)) and 15-minute streamflow at three USGS stream gages (i.e., Arroyo Seco NR Greenfield, CA (ID 11151870), Arroyo Seco NR Soledad, CA (ID 11152000), and Arroyo Seco BL Reliz C NR Soledad, CA (ID 11152050)) (Figure 1a). All data-model comparisons are performed at hourly-mean resolution.

4.2 Baseline simulation and soil moisture calibration

The model was run from January 1–31 of 2021. We performed the baseline simulation by modifying WRF-Hydro default parameters (Table S2) based on a calibration using soil moisture observations from stations lwd and gry. Neither PSL station is located in a burn scar. Since the baseline simulation includes no post-fire characteristics, it can also be regarded as the "pre-fire" scenario. Soil moisture at 10 cm below ground in the baseline simulation was calibrated by performing a domain-wide adjustment of soil porosity and grain size distribution index at the simulation start (Table S2). We then allowed the model to spin up from January 1–10 before using January 11–31 for validation.

After calibration, soil moisture closely mimics ground-based PSL observations (Figures 1c–d). Both observed magnitude and variability are well captured, with the simulated ±1 standard deviation envelope largely encompassing PSL observations during the AR. Model performance was evaluated using four quantitative metrics, i.e., correlation coefficient, root mean square error, mean bias, and the Kling-Gupta efficiency (KGE; Gupta et al., 2009) (Supporting Information Text S4)). The model's ability to simulate soil moisture substantially improves after calibration (Figures 1c–d; Table S3). KGE values approach 1 (0.72 at lwd and 0.88 at gry), indicating that WRF-Hydro adequately simulates the hydrologic environment and its response to meteorological change.

4.3 Burn scar simulation and streamflow calibration

To simulate effects of wildfire burn scars on hydrologic processes and debris-flow hazards, we made two modifications to the baseline simulation soil moisture calibrated model configuration. First, we changed the land cover type within the burn scar perimeter to its nearest LSM analogue, i.e., "barren and sparsely vegetated". Switch to barren land causes: (1) height of the canopy (HVT) to decrease to 0.5 m; (2) maximum rate of carboxylation at 25°C (VCMX25) to decrease to 0 $\mu mol\ CO_2/(m^2 \cdot s)$; and (3) overland flow roughness coefficient (OV_ROUGH2D) to decrease to 0.035 (Table S1 & Figures S5a–c) from default values (Supporting Information Text S2, Figure S3, and Table S1).

The second adjustment was to decrease soil infiltration rates within the burn scar perimeter, achieved by reducing soil saturated hydraulic conductivity (Figure S5d; Scott & van Wyk, 1990;

Cerdà, 1998; Robichaud, 2000; Martin & Moody, 2001) from default values (Table S2). Consistent with the hydrophobicity of burned soils, we calibrate the burn scar simulation by systematically exploring a range of burn scar area saturated hydraulic conductivities (0 to 3×10^{-7} m/s with a 5×10^{-8} m/s increment), with the goal of reproducing streamflow behavior similar to USGS gage observations. We found that a value of 1.5×10^{-7} m/s gives the highest Nash-Sutcliffe efficiency (NSE; Nash & Sutcliffe, 1970) (Supporting Information Text S4) across all three USGS stream gages (Table S3). NSEs increase from negative values in the baseline to greater than 0.5 when burn scar characteristics are included, and the NSEs at gages 1870 and 2000 reach 0.84 and 0.73, respectively. Higher NSE scores indicate the abovementioned burn scar parameter changes improve the model's ability to simulate streamflow observations (Table S3).

5 Results

5.1 Hydrologic response due to burn scar incorporation

The pre-fire baseline simulation fails to capture the hydrologic behavior observed at the USGS gage sites located within the burn scar (Figures 1e–g). Incorporation of burn scar characteristics substantially alters the hydrologic response of the model and provides much higher fidelity streamflow simulations (Figures 1e–g). Observed hydrographs are characterized by two early streamflow peaks related to two precipitation bursts on January 27th and 28th. Our burn scar simulation captures this behavior, while the baseline simulation streamflow peaks just once, with a lower magnitude and an ~3-day lag after peak precipitation (Figures 1e–g). The steep rising limbs and high magnitude discharge peaks of the burn scar hydrograph are indicative of flash flooding. Compared with the pre-fire baseline scenario, the burn scar's barren land and low infiltration rate substantially accelerate drainage rates and increase discharge volume into stream channels.

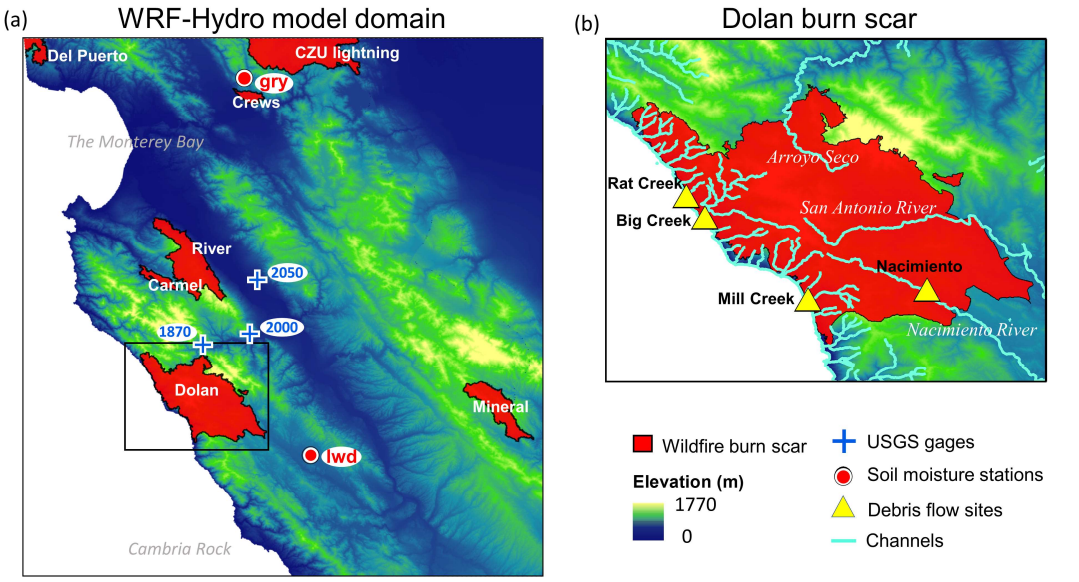
(a)
WRF-Hydro model domain
Del Puerto
CZU lightning
gry
Crews
The Monterey Bay
River
Carmel
2050
1870
2000
Dolan
Mineral
lwd
Cambria Rock
(b)
Dolan burn scar
Arroyo Seco
Rat Creek
San Antonio River
Big Creek
Nacimiento
Mill Creek
Nacimiento River
Wildfire burn scar
Elevation (m)
1770
0
USGS gages
Soil moisture stations
Debris flow sites
Channels

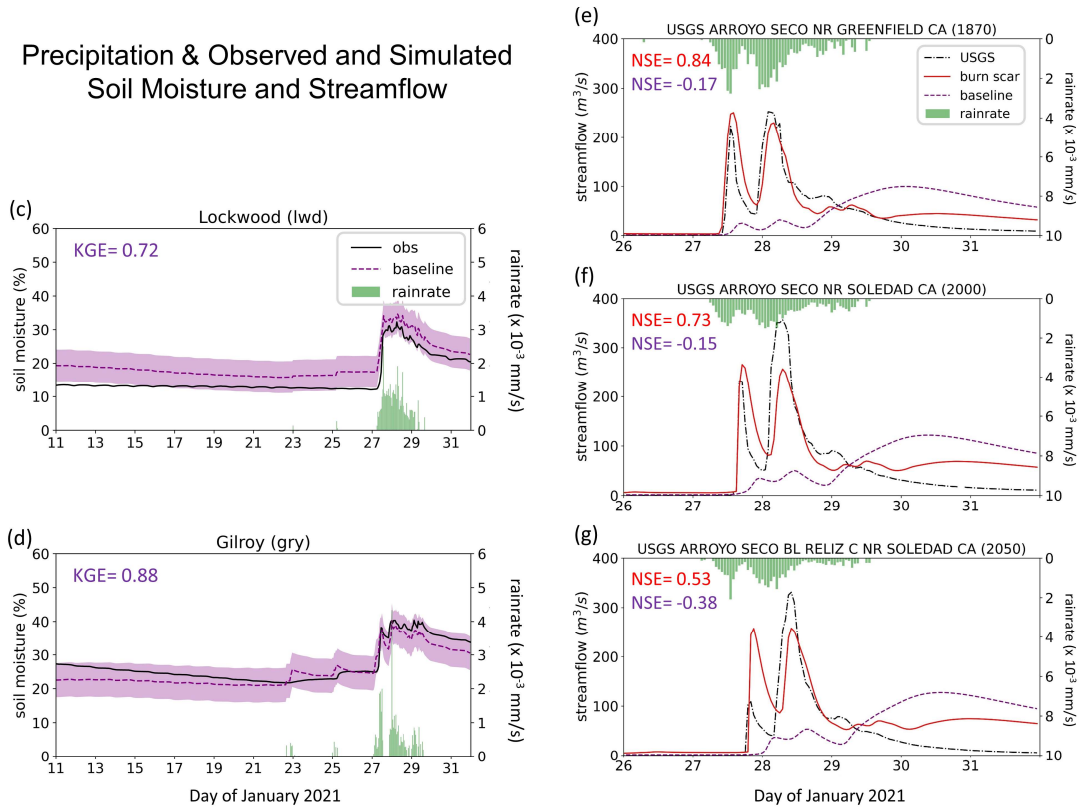
Precipitation & Observed and Simulated
Soil Moisture and Streamflow
(c)
Lockwood (lwd)
KGE= 0.72
obs
baseline
rainrate
soil moisture (%)
rainrate (x 10⁻³ mm/s)
(d)
Gilroy (gry)
KGE= 0.88
soil moisture (%)
rainrate (x 10⁻³ mm/s)
Day of January 2021
(e)
USGS ARROYO SECO NR GREENFIELD CA (1870)
NSE= 0.84
NSE= -0.17
USGS
burn scar
baseline
rainrate
streamflow (m³/s)
rainrate (x 10⁻³ mm/s)
(f)
USGS ARROYO SECO NR SOLEDAD CA (2000)
NSE= 0.73
NSE= -0.15
streamflow (m³/s)
rainrate (x 10⁻³ mm/s)
(g)
USGS ARROYO SECO BL RELIZ C NR SOLEDAD CA (2050)
NSE= 0.53
NSE= -0.38
streamflow (m³/s)
rainrate (x 10⁻³ mm/s)
Day of January 2021

Figure 1| WRF-Hydro study site with observed and simulated hydrologic conditions. (a) WRF-Hydro domain depicting topography, 2020 wildfire season burn scars, and PSL soil moisture and USGS stream gage observing sites. The black rectangle outlines the Dolan burn scar inset. (b) Dolan burn scar with debris flow locations and major streams. (c)–(d) January 11–31, 2021 MRMS precipitation and observed and simulated volumetric soil moisture 10 cm below ground at PSL sites (c) Lockwood (lwd) and (d) Gilroy (gry). Envelope of purple shading depicts ±1 standard deviation of model simulated soil moisture. KGE scores are provided at top left for each station. (e)–(g) January 26–31, 2021 MRMS precipitation, observed and baseline and burn scar simulated streamflow at three USGS gage sites. NSE scores for baseline and burn scar simulations are shown at top left.

5.2 Hydrologic response at four debris flow sites

We identified locations and extent of four debris flows from remote sensing data and field work (Figures 2a–d and Figure S2). rdNDVI shows vegetation loss caused by debris flows. Mill Creek, Big Creek, and Nacimiento were relatively large debris flows with runout lengths between ~2–5 km. Rat Creek occurred in a smaller catchment and had a runout length of ~300 m. The difference in runout length and debris-flow size is controlled by upstream catchment size. Due to its low stream order (1st Strahler stream order), Rat Creek is the only debris-flow site modeled entirely as overland flow in our WRF-Hydro simulations.

At the four debris-flow sites, we use three metrics to characterize hydrologic anomalies: (1) accumulated runoff volume, (2) peak discharge, and (3) time to peak discharge. Figures 2e–h depict accumulated channelized discharge volume (blue shading) and accumulated overland discharge volume (yellow-red shading) from January 27th 00:00 to 28th 12:00 near the four debris-flow sites in the burn scar simulation. Accumulation time period is chosen such that it covers the first two runoff surges in the simulated hydrographs which are likely associated with debris flows (Figures 2i–l) given that nearly concurrent peak rainfall intensity and peak discharge is a signature characteristic of debris flows (Kean et al., 2011). Runoff volume is on the order of 10^4 m^3 at Rat Creek and 10^6 m^3 at the other three sites.

Dramatic hydrographic changes after inclusion of burn scar characteristics are simulated at debris-flow source areas (Figure S6 and Table S4) and deposition sites (Figures 2i–l and Table S5). WRF-Hydro facilitates investigation of the hydrologic response at triggering and deposition locations and along the runout path. Here, to emphasize the downstream hazards, our analysis is focused on debris-flow deposits. At Rat Creek, where a section of CA1 collapsed, the magnitude of discharge substantially increases, and overland flow surges are concurrent with rainfall bursts (Figure 2i). Total discharge accumulated during the AR event increases approximately eight-fold, and peak discharge more than triples compared to the baseline simulation (Figure 2i and Table S5). At Mill Creek, Big Creek, and Nacimiento, baseline hydrographs are characterized by less variability, muted responses to two early precipitation bursts, and a delayed third discharge peak that does not

occur until ~3 days after AR passage (Figures 2j–l). Maximum discharge peaks in the baseline hydrographs lag those in the burn scar simulation by ~2 days (Figures 2j–l; Table S5). In the burn scar simulation, total volume substantially increases at the three channelized sites – total volume increases ~650% at Mill Creek, ~891% at Big Creek, and ~829% at Nacimiento (Figures 2j–l and Table S5), and the absolute increase in volume is on the order of 10^6 m^3 (Table S5). Peak discharge more than triples at Mill Creek and Big Creek and more than quadruples at Nacimiento. Additionally, response times of the peak in discharge to the peak in precipitation decrease to less than an hour, highlighting the simulated flashiness of the burned catchments.

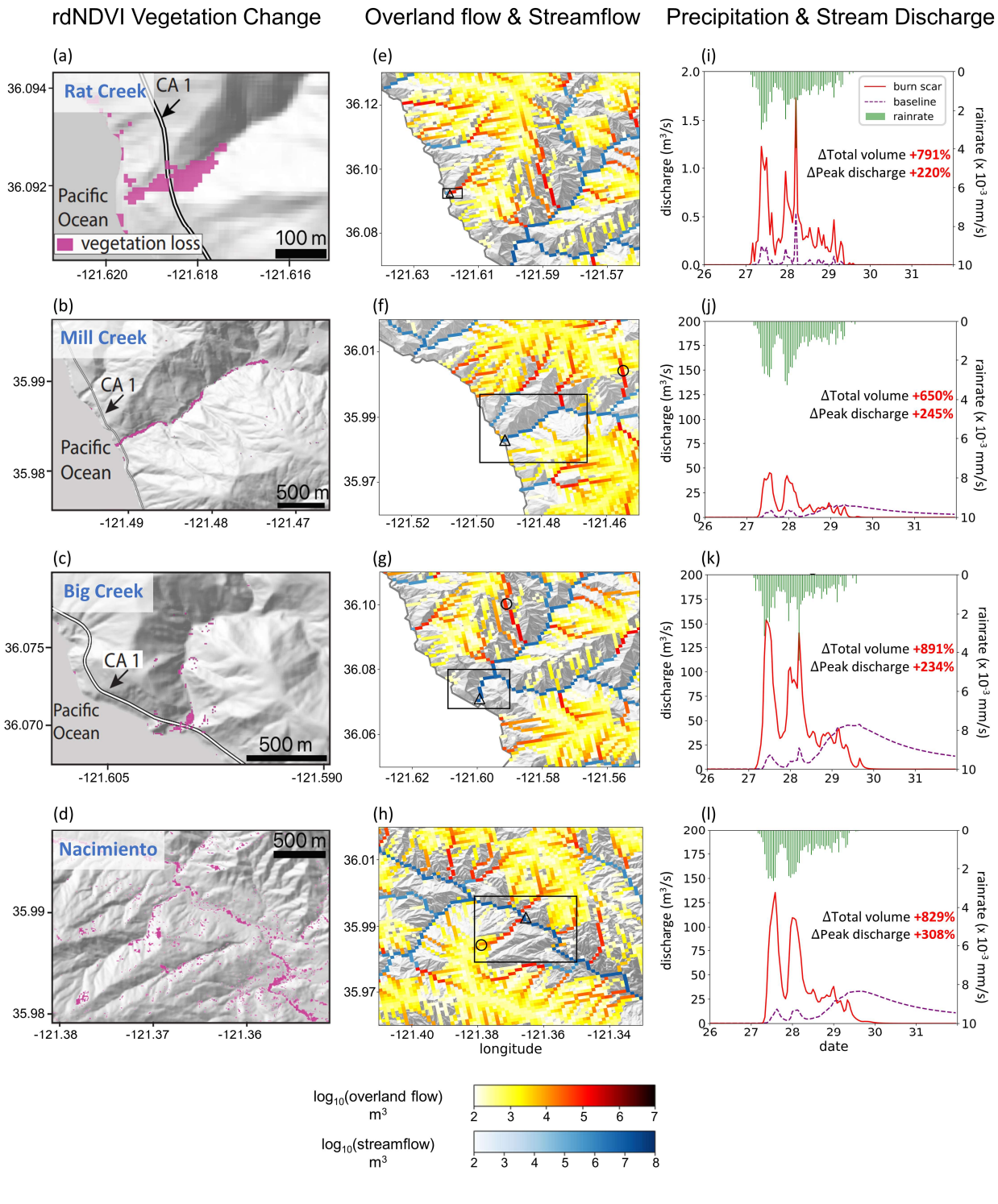
rdNDVI Vegetation Change
Overland flow & Streamflow
Precipitation & Stream Discharge
(a)
Rat Creek
CA 1
Pacific Ocean
vegetation loss
100 m
(b)
Mill Creek
CA 1
Pacific Ocean
500 m
(c)
Big Creek
CA 1
Pacific Ocean
500 m
(d)
Nacimiento
500 m
(e)
(f)
(g)
(h)
longitude
(i)
burn scar
baseline
rainrate
ΔTotal volume +791%
ΔPeak discharge +220%
(j)
ΔTotal volume +650%
ΔPeak discharge +245%
(k)
ΔTotal volume +891%
ΔPeak discharge +234%
(l)
ΔTotal volume +829%
ΔPeak discharge +308%
discharge (m³/s)
rainrate (x 10⁻³ mm/s)
date
log10(overland flow) m³
log10(streamflow) m³

Figure 2| Identified debris-flow sites and WRF-Hydro simulated discharge. (a)–(d) Sentinel-2 rdNDVI vegetation change at (a) Rat Creek, (b) Mill Creek, (c) Big Creek, and (d) Nacimiento. (e)–(h) Total volume of accumulated overland flow (yellow-red shading) and streamflow (blue shading) on log10 scale between January 27th 00:00 and 28th 12:00 at four debris-flow sites. Black rectangles correspond to domains of (a)–(d). Black circles and triangles indicate debris-flow source areas and deposits, respectively. (i)–(l) MRMS precipitation and baseline and burn scar simulated discharge time-series for January 26th 00:00 to 31st 23:00 at the four debris-flow deposition sites.

5.3 Debris-flow hazard assessment for the Dolan burn scar

Since high magnitude runoff is often the cause and precursor of runoff-generated debris flows in burned areas (Cannon et al., 2003, 2008; Rengers et al., 2016), we use simulated accumulated volume of overland flow and streamflow to assess runoff-generated debris-flow hazard potential under pre-fire (i.e., baseline; Figures 3a&d) and postfire (i.e., burn scar simulation; Figures 3b&e) conditions. We assess changes at both stream and catchment levels and use the difference between burn scar and baseline simulations to assess added debris-flow hazard potential (Figures 3c&f). Hazard levels are categorized according to the order of magnitude of runoff volume following USGS Emergency Assessment of Post-Fire Debris-Flow Hazards convention, i.e., low (0–10^3 m^3), medium (10^3–10^4 m^3), high (10^4–10^5 m^3), and very high (>10^5 m^3) (Figure 3; Cannon et al., 2010).

In the pre-fire simulation, the AR-induced precipitation produces a low debris-flow hazard over most of the domain, but medium-to-high hazards along stream channels (Figure 3a). We note no substantial differences between areas in or out of the burn scar. In the burn scar simulation, debris-flow hazard levels increase across the Dolan burn scar and along channels outside but downstream of the burn scar (Figures 3b–c). At Rat Creek, hazard levels increase from medium to high, while hazard levels at Big Creek, Mill Creek, and Nacimiento change from very high to beyond very high (above 10^6 m^3). Within the burn scar, hazard levels along major stream channels, such as the Nacimiento River and San Antonio River increase from high to very high. Outside the burn scar, hazard levels along river channels downstream of the burn scar, such as the Arroyo Seco River, also increase (Figure 3c).

At catchment level, debris-flow hazards are assessed using accumulated discharge volume at the outlet of each catchment between January 27th 00:00 to 28th 12:00 (Figures 3d–f). Corresponding normalized by catchment area hazard levels (Santi et al., 2012) are also provided (Figures 3g–i). In the baseline simulation, the majority of catchments are subject to low-to-medium debris-flow hazards (Figure 3d). In the burn scar simulation, over half of catchments within the Dolan burn scar have high-to-very high hazards, with over 1/3 of basins classified as having very high hazards (Figure 3e). Rat Creek catchment has a high hazard, while the three other sites are within catchments with very high hazards. The additional debris-flow hazard caused by the wildfire burn scar is substantial (Figure 3f). Beyond the burn scar perimeter, effects of fire expand to adjacent

and downstream catchments, and drainage basins of the Arroyo Seco and Nacimiento Rivers are simulated to have very high debris-flow hazards (Figures 3e&f). Catchment area-normalized hazard levels demonstrate that Mill Creek, Big Creek, and Nacimiento had above average hazard potential (Figures 3g–i), consistent with the event outcome.

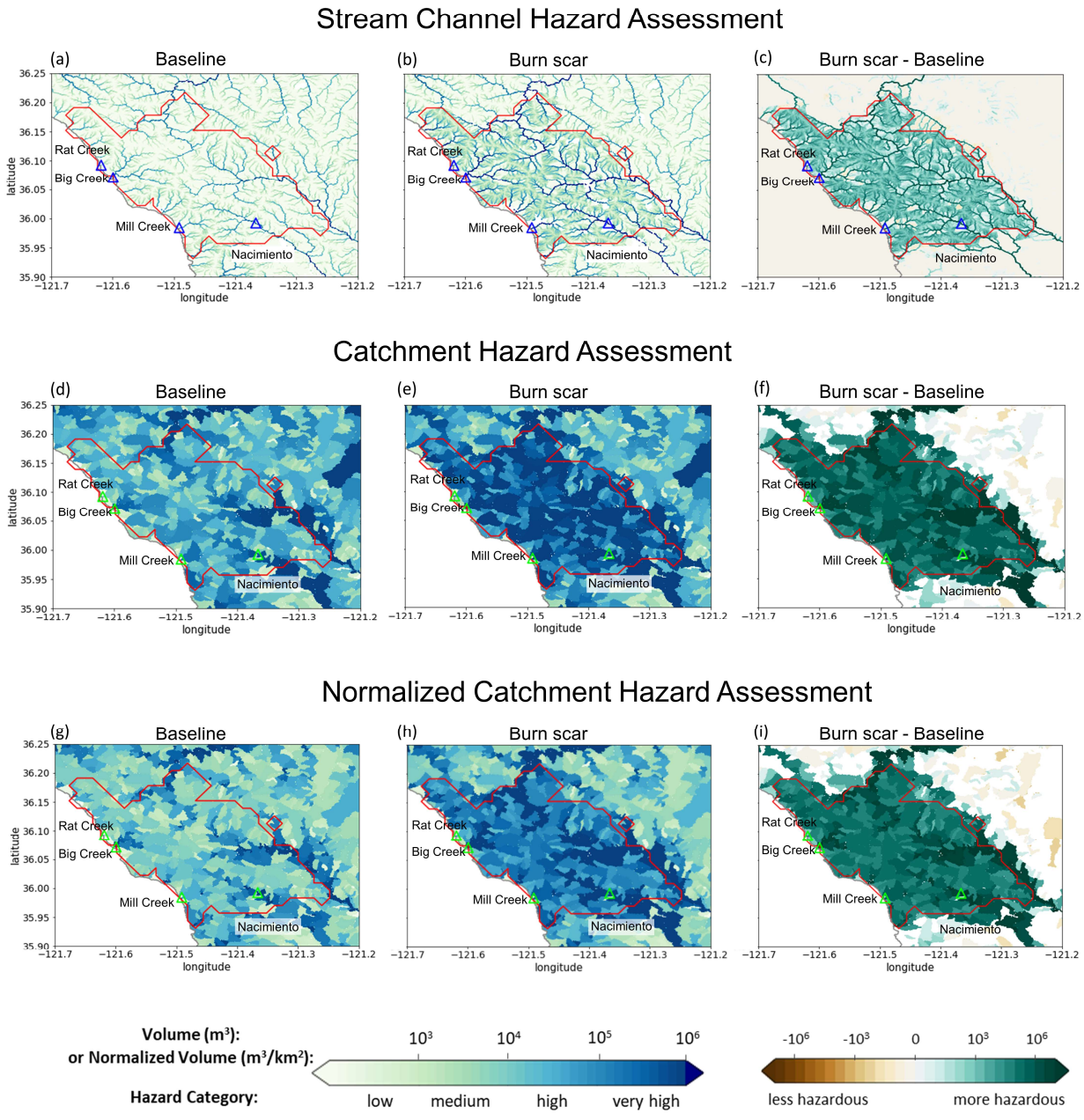

Figure 3| Runoff-generated debris-flow hazard levels. Hazard levels are categorized according to order of magnitude of overland flow and streamflow volume, i.e., low (0–10^3 m^3), medium (10^3–10^4 m^3), high (10^4–10^5 m^3), and very high (>10^5 m^3). Debris-flow hazards at individual stream level for the (a) baseline, (b) burn scar, and (c) difference between burn scar and baseline simulations. Hazard level is calculated as total discharge volume from January 27th 00:00 to 28th 12:00. (d)–(f) Debris-flow hazards at catchment level. For each catchment, the hazard is determined by total discharge volume at the catchment outlet from January 27th 00:00 to 28th 12:00. (g)–(i) Debris-flow hazards normalized by catchment area.

6 Discussion and conclusion

Given the historic and growing frequency of wildfires in the western U.S. (Swain 2021; Williams et al., 2019; Goss et al., 2020) and globally (Jolly et al., 2015; Flannigan et al., 2013), developing tools to investigate, better understand, and potentially predict changes in burn scar hydrology and natural hazards is critical. Here, we demonstrate the first use of WRF-Hydro to simulate the surface hydrologic response over a burn scar during a landfalling AR. We modified the default WRF-Hydro to output overland flow and to replicate burn scar behavior by adjusting vegetation type and infiltration rate parameters. WRF-Hydro simulations were validated against PSL soil moisture and USGS streamflow observations before we used simulated streamflow and overland flow volumes to characterize debris-flow hazard potential. A comparison between baseline and burn scar simulations demonstrated that changes in hydraulic properties of burned areas causes drastic changes in surface flows, including faster discharge response times, greater discharge volumes, and overall flashier hydrologic behavior in surface flows. The magnitude of our simulated changes is consistent with findings from previous postfire hydrology studies (Anderson et al., 1976; Scott, 1993; Meixner & Wohlgemuth, 2003; Kinoshita & Hogue, 2015; Kean et al., 2011). At Rat Creek, where a debris flow destroyed CA1, our model simulation predicted an eight-fold increase in accumulated overland flow and a tripling in peak discharge when compared to the baseline simulation. At Mill Creek, Big Creek, and Nacimiento, runoff volume in the burn scar simulation is on the order of 10^6 m^3 which the USGS categorizes as a very high debris-flow hazard (Cannon et al., 2010).

Despite methodological differences, our debris-flow hazard assessment for this AR event is generally consistent with the USGS' post-fire, pre-AR, design-storm-based preliminary hazard assessment (USGS, 2020). USGS preliminary hazard assessments use logistic regression models to estimate the likelihood of debris-flow occurrence and multivariate linear regression models to estimate debris-flow volumes. This empirical approach is trained on historical western U.S. debris-flow occurrence and magnitude data and incorporates estimated burn scar soil erodibility and burn severity data (Cannon et al., 2010; Gartner et al., 2014; Staley et al., 2016). For the Dolan burn scar, both assessments find that (*i*) large stream channels had relatively higher hazard levels than small streams or overland areas, (*ii*) almost the entire burn scar had medium hazard and above,

and (*iii*) approximately half of burn scar catchments were subject to high-to-very high debris-flow hazards. However, close comparison of hazard maps reveals differences in spatial distribution of high-hazard catchments. In the USGS assessment, higher hazard levels are predicted north and southeast of the burn scar, whereas in our assessment the highest hazards occur along major stream channels. We hypothesize that USGS-assessed areas of higher hazard potential are related to their use of design-storm precipitation (see Figure S1 for MRMS precipitation footprint) and burn severity data (Burned Area Emergency Response, 2020). Comparison with the USGS assessment framework suggests room for improvement in WRF-Hydro-based assessments (i.e., inclusion of burn severity and soil erodibility data), but also highlights the potential utility of working with spatially-distributed and time-varying precipitation.

As a water-only model, WRF-Hydro is currently restricted to simulating the hydrologic ingredients of debris flows. While water-only models have been widely used to investigate and better understand debris-flow dynamics (Arattano & Savage, 1994; Arattano & Franzi, 2010; Rengers et al., 2016; McGuire & Youberg, 2020; Di Cristo et al., 2021), sediment supply, soil erodibility, and other sedimentological factors also play important roles in determining the potential for and severity of mass failure events (McGuire et al., 2017). Developing a debris-flow model that couples hydrologic and sediment erosion and transport processes would represent a significant advance and be of great practical use (Banihabib et al., 2020; Shen et al., 2021). At a minimum, soil grain size maps and domain-specific rainfall intensity-duration curves can provide guidance to define transitions from water floods to debris flows (McGuire & Youberg, 2020; Tognacca et al., 2000; Gregoretti & Fontana, 2008; Cannon et al., 2007).

Use of WRF-Hydro to simulate runoff-generated debris-flow hazards in burn scar settings represents a novel application. Other potential applications of our modified model framework include alpine areas and steep hillslopes with sparse vegetation where runoff-generated debris flows dominate over landslide-initiated ones (Davies et al., 1992; Coe et al., 2003, 2008). In addition, here WRF-Hydro is driven by historical precipitation and meteorological data, i.e., hindcast mode. We see no reason why this modeling framework could not also be employed to project hazards under future climatic conditions (e.g., Huang et al., 2020), or given its relatively low computational expense, in operational forecast mode. Indeed, modern ensemble-based meteorological forecasting could provide high spatiotemporal forcing data with which disaster preparedness managers could probabilistically assess debris-flow hazard potential, and issue advanced life and property saving warnings.

Acknowledgments

C.L., A.L.H., J.W., X.L., G.B., and D.E.H. acknowledge support from NSF PREEVENTS #1848683. We acknowledge high-performance computing support from Cheyenne (doi:10.5065/D6RX99HX) provided by NCAR's Computational and Information Systems Laboratory, sponsored by the National Science Foundation.

Data availability statement

The NLDAS-2 reanalysis forcing data is publicly available at NASA GES DISC: https://disc.gsfc.nasa.gov/datasets?keywords=NLDAS. A detailed description can be found at https://ldas.gsfc.nasa.gov/nldas/v2/forcing. The MRMS radar-only precipitation estimate is publicly available at: https://mtarchive.geol.iastate.edu/. A description can be found at https://www.nssl.noaa.gov/projects/mrms/. The PSL in-situ soil moisture data is publicly available at: https://psl.noaa.gov/data/obs/datadisplay/. The USGS streamflow is publicly available at: https://waterdata.usgs.gov/nwis/.

The remote sensing data used in this manuscript were provided by the European Space Agency (ESA) Copernicus program and accessed on Google Earth Engine (https://code.earthengine.google.com).

All processed data required to reproduce the results of this study are archived on Zenodo at http://doi.org/10.5281/zenodo.5544083.

Code availability statement

The modified WRF-Hydro Fortran code and instructions to output the overland flow at terrain routing grid can be downloaded at https://github.com/NU-CCRG/Modified-WRF-Hydro.

HazMapper v1.0 is available at https://hazmapper.org/. The SAR backscatter change method code is available at https://github.com/MongHanHuang/GEE_SAR_landslide_detection.

References

Anderson, H. W., Hoover, M. D., & Reinhart, K. G. (1976). Forests and water: effects of forest management on floods, sedimentation, and water supply (Vol. 18): Department of Agriculture, Forest Service, Pacific Southwest Forest and Range Experiment Station, Berkeley, CA.

Arattano, M., & Franzi, L. (2010). On the application of kinematic models to simulate the diffusive processes of debris flows. Nat. Hazards Earth Syst. Sci., 10(8), 1689-1695. doi:10.5194/nhess-10-1689-2010

Arattano, M., & Savage, W. Z. J. B. o. t. I. A. o. E. G.-B. d. l. A. I. d. G. d. l. I. (1994). Modelling debris flows as kinematic waves. 49, 3-13.

Banihabib, M. E., Jurik, L., Kazemi, M. S., Soltani, J., & Tanhapour, M. (2020). A Hybrid Intelligence Model for the Prediction of the Peak Flow of Debris Floods. Water, 12(8). doi:10.3390/w12082246

Bart, R. (2016). A regional estimate of postfire streamflow change in California. Water Resources Research, 52, n/a-n/a. doi:10.1002/2014WR016553

Bart, R., & Hope, A. (2010). Streamflow response to fire in large catchments of a Mediterranean-climate region using paired-catchment experiments. Journal of Hydrology, 388, 370-378. doi:10.1016/j.jhydrol.2010.05.016

Brown, E.K., J. Wang, and Yan Feng. 2020. U.S. wildfire potential: a historical view and future projection using high-resolution climate data. Environmental Research Letters. 16, 034060

Camera, C., Bruggeman, A., Zittis, G., Sofokleous, I., & Arnault, J. (2020). Simulation of extreme rainfall and streamflow events in small Mediterranean watersheds with a one-way-coupled atmospheric-hydrologic modelling system. Natural hazards and earth system sciences, 20(10), 2791-2810. doi:10.5194/nhess-20-2791-2020

Canfield, H., Goodrich, D., & Burns, I. S. (2005). Selection of Parameters Values to Model Post-Fire Runoff and Sediment Transport at the Watershed Scale in Southwestern Forests.

Cannon, S., Gartner, J., C, P., & Parise, M. (2003). Widlfire-related debris-flow generation through episodic progressive sediment-bulking processes, western USA (Vol. 1).

Cannon, S., Gartner, J., Wilson, R., Bowers, J., & Laber, J. (2008). Storm Rainfall Conditions for Floods and Debris Flows from Recently Burned Basins in Southwestern Colorado and Southern California. Geomorphology, 96, 250-269. doi:10.1016/j.geomorph.2007.03.019

Cannon, S. H. (2001). Debris-flow generation from recently burned watersheds. Environmental & Engineering Geoscience, 7(4), 321-341.

Cannon, S. H., Boldt, E. M., Laber, J. L., Kean, J. W., & Staley, D. M. J. N. H. (2011). Rainfall intensity–duration thresholds for postfire debris-flow emergency-response planning. 59(1), 209-236.

Cannon, S. H., & DeGraff, J. (2009). The increasing wildfire and post-fire debris-flow threat in western USA, and implications for consequences of climate change. In Landslides–disaster risk reduction (pp. 177-190): Springer.

Cannon, S. H., Gartner, J. E., Rupert, M. G., Michael, J. A., Rea, A. H., & Parrett, C. (2010). Predicting the probability and volume of postwildfire debris flows in the intermountain western United States. GSA Bulletin, 122(1-2), 127-144. doi:10.1130/B26459.1

Cerdà, A. (1998). Changes in overland flow and infiltration after a rangeland fire in a Mediterranean scrubland. Hydrological Processes, 12(7), 1031-1042. doi:https://doi.org/10.1002/(SICI)1099-1085(19980615)12:7<1031::AID-HYP636>3.0.CO;2-V

Chen, L., Berli, M., & Chief, K. (2013). Examining Modeling Approaches for the Rainfall-Runoff Process in Wildfire-Affected Watersheds: Using San Dimas Experimental Forest. JAWRA Journal of the American Water Resources Association, 49(4), 851-866. doi:https://doi.org/10.1111/jawr.12043

Reynolds, C., (2021, February 25). Highway 1 washout near Big Sur expected to be fixed by summer, Los Angeles Times. https://www.latimes.com/travel/story/2021-02-25/highway-1-to-big-sur-will-reopen-by-summer-caltrans-says

Coe, J., Godt, J., Parise, M., & Moscariello, A. (2003). Estimating debris-flow probability using fan stratigraphy, historic records, and drainage-basin morphology, Interstate 70 highway corridor, central Colorado, USA. Paper presented at the Debris-Flow Hazards Mitigation: Mechanics, Prediction, and

Assessment, edited by: Rickenmann, D. and Cheng, Ch., Proceedings 3rd International DFHM Conference, Davos, Switzerland.
Coe, J. A., Kinner, D. A., & Godt, J. W. J. G. (2008). Initiation conditions for debris flows generated by runoff at Chalk Cliffs, central Colorado. 96(3-4), 270-297.
Cydzik, K., & Hogue, T. S. J. J. J. o. t. A. W. R. A. (2009). Modeling postfire response and recovery using the hydrologic engineering center hydrologic modeling system (HEC-HMS) 1. 45(3), 702-714.
Davies, T., Phillips, C., Pearce, A., & Zhang, X. J. I. P. (1992). Debris flow behaviour–an integrated overview. 209(21), 225.
Dekker, L. W., & Ritsema, C. J. (1994). How water moves in a water repellent sandy soil: 1. Potential and actual water repellency. Water Resources Research, 30(9), 2507-2517. doi:https://doi.org/10.1029/94WR00749
Di Cristo, C., Iervolino, M., Moramarco, T., & Vacca, A. (2021). Applicability of Diffusive model for mud-flows: An unsteady analysis. Journal of Hydrology, 600, 126512. doi:https://doi.org/10.1016/j.jhydrol.2021.126512
Doerr, S. H., & Thomas, A. (2000). The role of soil moisture in controlling water repellency: New evidence from forest soils in Portugal. Journal of Hydrology, 231-232, 134-147. doi:10.1016/S0022-1694(00)00190-6
Gartner, J. E., Cannon, S. H., & Santi, P. M. (2014). Empirical models for predicting volumes of sediment deposited by debris flows and sediment-laden floods in the transverse ranges of southern California. Engineering Geology, 176, 45-56. doi:https://doi.org/10.1016/j.enggeo.2014.04.008
George, D. L., & Iverson, R. M. (2014). A depth-averaged debris-flow model that includes the effects of evolving dilatancy. II. Numerical predictions and experimental tests. Proceedings of the Royal Society A: Mathematical, Physical and Engineering Sciences, 470(2170), 20130820. doi:10.1098/rspa.2013.0820
Goodrich, D., Burns, I., Unkrich, C., Semmens, D., Guertin, D., Hernandez, M., . . . Levick, L. (2012). KINEROS2/AGWA: model use, calibration, and validation. Transactions of the ASABE, 55, 1561-1574. doi:10.13031/2013.42264
Goss, M., Swain, D. L., Abatzoglou, J. T., Sarhadi, A., Kolden, C. A., Williams, A. P., & Diffenbaugh, N. S. (2020). Climate change is increasing the likelihood of extreme autumn wildfire conditions across California. Environmental Research Letters, 15(9), 094016. doi:10.1088/1748-9326/ab83a7
Gregoretti, C., & Fontana, G. D. (2008). The triggering of debris flow due to channel-bed failure in some alpine headwater basins of the Dolomites: analyses of critical runoff. Hydrological Processes, 22(13), 2248-2263. doi:https://doi.org/10.1002/hyp.6821
Gupta, H. V., Kling, H., Yilmaz, K. K., & Martinez, G. F. (2009). Decomposition of the mean squared error and NSE performance criteria: Implications for improving hydrological modelling. Journal of Hydrology, 377(1), 80-91. doi:https://doi.org/10.1016/j.jhydrol.2009.08.003
Handwerger, A. L., Jones, S. Y., Amatya, P., Kerner, H. R., Kirschbaum, D. B., and Huang, M.-H. (in review): Strategies for landslide detection using open-access synthetic aperture radar backscatter change in Google Earth Engine, Nat. Hazards Earth Syst. Sci. Discuss.
Huang, X., Swain, D. L., & Hall, A. D. (2020). Future precipitation increase from very high resolution ensemble downscaling of extreme atmospheric river storms in California. 6(29), eaba1323. doi:10.1126/sciadv.aba1323 %J Science Advances

Ice, G. G., Neary, D. G., & Adams, P. W. (2004). Effects of Wildfire on Soils and Watershed Processes. Journal of Forestry, 102(6), 16-20. doi:10.1093/jof/102.6.16

Iverson, R. M., & George, D. L. (2014). A depth-averaged debris-flow model that includes the effects of evolving dilatancy. I. Physical basis. Proceedings of the Royal Society A: Mathematical, Physical and Engineering Sciences, 470(2170), 20130819. doi:10.1098/rspa.2013.0819

Jolly, W. M., Cochrane, M. A., Freeborn, P. H., Holden, Z. A., Brown, T. J., Williamson, G. J., & Bowman, D. M. J. S. (2015). Climate-induced variations in global wildfire danger from 1979 to 2013. Nature Communications, 6(1), 7537. doi:10.1038/ncomms8537

Julien, P. Y., Saghafian, B., & Ogden, F. L. (1995). RASTER-BASED HYDROLOGIC MODELING OF SPATIALLY-VARIED SURFACE RUNOFF1. JAWRA Journal of the American Water Resources Association, 31(3), 523-536. doi:https://doi.org/10.1111/j.1752-1688.1995.tb04039.x

Kean, J. W., McCoy, S. W., Tucker, G. E., Staley, D. M., & Coe, J. A. (2013). Runoff-generated debris flows: Observations and modeling of surge initiation, magnitude, and frequency. Journal of Geophysical Research: Earth Surface, 118(4), 2190-2207. doi:https://doi.org/10.1002/jgrf.20148

Kean, J. W., & Staley, D. M. (2021). Forecasting the Frequency and Magnitude of Postfire Debris Flows Across Southern California. Earth's Future, 9(3), e2020EF001735. doi:https://doi.org/10.1029/2020EF001735

Kean, J. W., Staley, D. M., & Cannon, S. H. (2011). In situ measurements of post-fire debris flows in southern California: Comparisons of the timing and magnitude of 24 debris-flow events with rainfall and soil moisture conditions. Journal of Geophysical Research F: Earth Surface, 116(4). doi:10.1029/2011JF002005

Kinoshita, A. M., & Hogue, T. S. (2015). Increased dry season water yield in burned watersheds in Southern California. Environmental Research Letters, 10(1), 014003. doi:10.1088/1748-9326/10/1/014003

Larsen, I., MacDonald, L., Brown, E., Rough, D., Welsh, M., Pietraszek, J., . . . Schaffrath, K. (2009). Causes of Post-Fire Runoff and Erosion: Water Repellency, Cover, or Soil Sealing? Soil Science Society of America Journal - SSSAJ, 73. doi:10.2136/sssaj2007.0432

Lahmers, T. M., Castro, C. L., & Hazenberg, P. (2020). Effects of Lateral Flow on the Convective Environment in a Coupled Hydrometeorological Modeling System in a Semiarid Environment, Journal of Hydrometeorology, 21(4), 615-642. Retrieved Sep 29, 2021, from https://journals.ametsoc.org/view/journals/hydr/21/4/jhm-d-19-0100.1.xml

MacDonald, L. H., & Huffman, E. L. (2004). Post-fire soil water repellency: Persistence and soil moisture thresholds. Soil Science Society of America Journal, 68, 1729-1734.

Martin, D., & Moody, J. (2001). Comparison of Soil Infiltration Rates in Burned and Unburned Mountainous Watersheds. Hydrological Processes, 15, 2893-2903. doi:10.1002/hyp.380

McGuire, L. A., Rengers, F. K., Kean, J. W., & Staley, D. M. (2017). Debris flow initiation by runoff in a recently burned basin: Is grain-by-grain sediment bulking or en masse failure to blame? Geophysical Research Letters, 44(14), 7310-7319. doi:https://doi.org/10.1002/2017GL074243

McGuire, L. A., & Youberg, A. M. (2020). What drives spatial variability in rainfall intensity-duration thresholds for post-wildfire debris flows? Insights from the 2018 Buzzard Fire, NM, USA. Landslides, 17(10), 2385-2399. doi:10.1007/s10346-020-01470-y

McMichael, C. E., & Hope, A. S. (2007). Predicting streamflow response to fire-induced landcover change: implications of parameter uncertainty in the MIKE SHE model. J Environ Manage, 84(3), 245-256. doi:10.1016/j.jenvman.2006.06.003

Meixner, T., & Wohlgemuth, P. (2003). Climate Variability, Fire, Vegetation Recovery, and Watershed Hydrology.

Meyer, G. A., & Wells, S. G. (1997). Fire-related sedimentation events on alluvial fans, Yellowstone National Park, U.S.A. Journal of Sedimentary Research, 67(5), 776-791. doi:10.1306/D426863A-2B26-11D7-8648000102C1865D

Mikoš, M., & Bezak, N. (2021). Debris Flow Modelling Using RAMMS Model in the Alpine Environment With Focus on the Model Parameters and Main Characteristics. 8(732). doi:10.3389/feart.2020.605061

Moody, J., & Ebel, B. (2012). Hyper-dry conditions provide new insights into the cause of extreme floods after wildfire. CATENA, 93, 58-63. doi:10.1016/j.catena.2012.01.006

Moody, J., Shakesby, R., Robichaud, P., Cannon, S., & Martin, D. A. J. E.-S. R. (2013). Current research issues related to post-wildfire runoff and erosion processes. 122, 10-37.

Nash, J. E., & Sutcliffe, J. V. (1970). River flow forecasting through conceptual models part I — A discussion of principles. Journal of Hydrology, 10(3), 282-290. doi:https://doi.org/10.1016/0022-1694(70)90255-6

Neary, D., Gottfried, G., & Ffolliott, P. (2003). Post-wildfire watershed flood responses.

Niu G-Y et al. (2011) The community Noah land surface model with multiparameterization options (Noah-MP): 1. Model description and evaluation with local-scale measurements J Geophys Res Atm 116 doi:https://doi.org/10.1029/2010JD015139

Nyman, P., Smith, H. G., Sherwin, C. B., Langhans, C., Lane, P. N. J., & Sheridan, G. J. (2015). Predicting sediment delivery from debris flows after wildfire. Geomorphology, 250, 173-186. doi:https://doi.org/10.1016/j.geomorph.2015.08.023

Oakley, N. S. (2021). A warming climate adds complexity to post-fire hydrologic hazard planning. Earth's Future, 9, e2021EF002149. https://doi.org/10.1029/2021EF002149

Ogden, F. L. J. D. o. C., & Environmental Engineering, U. o. C., Storrs. (1997). CASC2D reference manual.

Polade SD, Gershunov A, Cayan DR, Dettinger MD, Pierce DW (2017) Precipitation in a warming world: Assessing projected hydro-climate changes in California and other Mediterranean climate regions Scientific Reports 7:10783 doi:10.1038/s41598-017-11285-y

Rengers, F. K., McGuire, L. A., Kean, J. W., Staley, D. M., & Hobley, D. E. J. (2016). Model simulations of flood and debris flow timing in steep catchments after wildfire. Water Resources Research, 52(8), 6041-6061. doi:https://doi.org/10.1002/2015WR018176

Robichaud, P., Beyers, J., & Neary, D. (2000). Evaluating the effectiveness of postfire rehabilitation treatments.

Rulli, M. C., & Rosso, R. (2007). Hydrologic response of upland catchments to wildfires. Advances in Water Resources, 30(10), 2072-2086. doi:https://doi.org/10.1016/j.advwatres.2006.10.012

Santi, P. M., deWolfe, V. G., Higgins, J. D., Cannon, S. H., & Gartner, J. E. (2008). Sources of debris flow material in burned areas. Geomorphology, 96(3-4), 310-321. doi:10.1016/j.geomorph.2007.02.022

Santi, P. M., & Morandi, L. (2013). Comparison of debris-flow volumes from burned and unburned areas. Landslides, 10(6), 757-769.

Scheip, C. M., & Wegmann, K. W. (2021). HazMapper: A global open-source natural hazard mapping application in Google Earth Engine. Natural Hazards and Earth System Sciences, 21(5), 1495-1511.

Scott, D. F., & Van Wyk, D. B. (1990). The effects of wildfire on soil wettability and hydrological behaviour of an afforested catchment. 121, 239. doi:10.1016/0022-1694(90)90234-o

Scott, D. J. J. o. H. (1993). The hydrological effects of fire in South African mountain catchments. 150, 409-432.

Shakesby, R. A., & Doerr, S. H. (2006). Wildfire as a hydrological and geomorphological agent. Earth-Science Reviews, 74(3), 269-307. doi:https://doi.org/10.1016/j.earscirev.2005.10.006

Shen H, Lynch B, Poulsen CJ, Yanites BJ (2021) A modeling framework (WRF-Landlab) for simulating orogen-scale climate-erosion coupling Computers & Geosciences 146:104625 doi:https://doi.org/10.1016/j.cageo.2020.104625

Sidman, G., Guertin, D., Goodrich, D., Unkrich, C., & Burns, I. (2016). Risk assessment of post-wildfire hydrological response in semiarid basins: the effects of varying rainfall representations in the KINEROS2/AGWA model. International Journal of Wildland Fire, 25, 268-278. doi:10.1071/WF14071

Staley, D. M., Negri, J. A., Kean, J. W., Laber, J. L., Tillery, A. C., & Youberg, A. M. (2016). Updated logistic regression equations for the calculation of post-fire debris-flow likelihood in the western United States (2016-1106). Retrieved from Reston, VA: http://pubs.er.usgs.gov/publication/ofr20161106

Stoof, C. R., Vervoort, R. W., Iwema, J., van den Elsen, E., Ferreira, A. J. D., & Ritsema, C. J. (2012). Hydrological response of a small catchment burned by experimental fire. Hydrol. Earth Syst. Sci., 16(2), 267-285. doi:10.5194/hess-16-267-2012

Swain, D. L. (2021). A Shorter, Sharper Rainy Season Amplifies California Wildfire Risk. Geophysical Research Letters, 48(5), e2021GL092843. doi:https://doi.org/10.1029/2021GL092843

Swain DL, Langenbrunner B, Neelin JD, Hall A (2018) Increasing precipitation volatility in twenty-first-century California Nature Climate Change 8:427-433 doi:10.1038/s41558-018-0140-y

Tognacca, C., Bezzola, G., & Minor, H.-E. (2000). Threshold criterion for debris-flow initiation due to channel-bed failure. Paper presented at the Debris-flow hazards mitigation: Mechanics, prediction and assessment.

U.S. Forest Service, Burned Area Emergency Response, Dolan Post-fire BAER Soil Burn Severity Map Released, October 10, 2020, https://inciweb.nwcg.gov/photos/CALPF/2020-10-06-1821-Dolan-PostFire-BAER/related_files/pict20200910-143346-0.pdf

U.S. Forest Service, Burned Area Emergency Response, Dolan Fire Burned Area Report, October 13, 2020, https://inciweb.nwcg.gov/photos/CALPF/2020-10-06-1821-Dolan-PostFire-BAER/related_files/pict20200927-132609-0.pdf

U.S. Geological Survey, Post-Fire Debris-Flow Hazards: Dolan Fire (Los Padres National Forest, CA), Landslide Hazards Program, retrieved September 27, 2021, from https://landslides.usgs.gov/hazards/postfire_debrisflow/detail.php?objectid=312

Wang, J., Wang, C., Rao, V., Orr, A., Yan, E., & Kotamarthi, R. (2019). A parallel workflow implementation for PEST version 13.6 in high-performance computing for WRF-Hydro version 5.0: a case study over the midwestern United States. Geoscientific Model Development, 12(8), 3523-3539. doi:10.5194/gmd-12-3523-2019

Williams, A. P., Abatzoglou, J. T., Gershunov, A., Guzman-Morales, J., Bishop, D. A., Balch, J. K., & Lettenmaier, D. P. (2019). Observed Impacts of Anthropogenic Climate Change on Wildfire in California. Earth's Future, 7(8), 892-910. doi:https://doi.org/10.1029/2019EF001210

References From the Supporting Information

Andersson, J. C. M., Arheimer, B., Traoré, F., Gustafsson, D., & Ali, A. (2017). Process refinements improve a hydrological model concept applied to the Niger River basin. Hydrological Processes, 31(25), 4540-4554. doi:https://doi.org/10.1002/hyp.11376

Bitew, M. M., & Gebremichael, M. (2011). Assessment of satellite rainfall products for streamflow simulation in medium watersheds of the Ethiopian highlands. Hydrol. Earth Syst. Sci., 15(4), 1147-1155. doi:10.5194/hess-15-1147-2011

Chen, F., & Dudhia, J. (2001). Coupling an Advanced Land Surface? Hydrology Model with the Penn State?NCAR MM5 Modeling System. Part I: Model Implementation and Sensitivity. Monthly Weather Review, 129(4), 569-585. doi:10.1175/1520-0493(2001)129<0569:CAALSH>2.0.CO;2

Cosby, B. J., Hornberger, G. M., Clapp, R. B., & Ginn, T. R. (1984). A Statistical Exploration of the Relationships of Soil Moisture Characteristics to the Physical Properties of Soils. Water Resources Research, 20(6), 682-690. doi:https://doi.org/10.1029/WR020i006p00682

Kling, H., Fuchs, M., & Paulin, M. (2012). Runoff conditions in the upper Danube basin under an ensemble of climate change scenarios. Journal of Hydrology, 424-425, 264-277. doi:https://doi.org/10.1016/j.jhydrol.2012.01.011

Lahmers, T. M., Gupta, H., Castro, C. L., Gochis, D. J., Yates, D., Dugger, A., . . . Hazenberg, P. J. J. o. H. (2019). Enhancing the structure of the WRF-Hydro hydrologic model for semiarid environments. 20(4), 691-714.

Miller, D. A., & White, R. A. (1998). A Conterminous United States Multilayer Soil Characteristics Dataset for Regional Climate and Hydrology Modeling, Earth Interactions, 2(2), 1-26. Retrieved Sep 27, 2021, from https://journals.ametsoc.org/view/journals/eint/2/2/1087-3562_1998_002_0001_acusms_2.3.co_2.xml

N. Moriasi, D., G. Arnold, J., W. Van Liew, M., L. Bingner, R., D. Harmel, R., & L. Veith, T. (2007). Model Evaluation Guidelines for Systematic Quantification of Accuracy in Watershed Simulations. Transactions of the ASABE, 50(3), 885-900. doi:https://doi.org/10.13031/2013.23153

Schaefli, B., & Gupta, H. V. (2007). Do Nash values have value? Hydrological Processes, 21(15), 2075-2080. https://doi.org/10.1002/hyp.6825

Schönfelder, L., Bakken, T., Alfredsen, K., & Adera, A. (2017). Application of HYPE in Norway.

Vergopolan, N., Chaney, N. W., Beck, H. E., Pan, M., Sheffield, J., Chan, S., & Wood, E. F. (2020). Combining hyper-resolution land surface modeling with SMAP brightness temperatures to obtain 30-m soil moisture estimates. Remote Sensing of Environment, 242, 111740. doi:https://doi.org/10.1016/j.rse.2020.111740

Xia, Y., Mitchell, K., Ek, M., Cosgrove, B., Sheffield, J., Luo, L., . . . Lohmann, D. (2012). Continental-scale water and energy flux analysis and validation for North American Land Data Assimilation System project phase 2 (NLDAS-2): 2. Validation of model-simulated streamflow. Journal of Geophysical Research: Atmospheres, 117(D3). doi:https://doi.org/10.1029/2011JD016051